

Electronic Supplementary Information (ESI)

## **Local Orientation of Chains at Crystal/Amorphous Interfaces Buried in Isotactic Polypropylene Thin Films**

Daisuke Kawaguchi<sup>1,2\*</sup>, Kentaro Yamamoto<sup>1</sup>, Tatsuki Abe<sup>1</sup>, Naisheng Jiang<sup>3</sup>,  
Tadanori Koga<sup>3,4</sup>, Satoru Yamamoto<sup>2</sup>, and Keiji Tanaka<sup>1,2,5\*</sup>

<sup>1</sup> Department of Applied Chemistry, Kyushu University, Fukuoka, Japan

<sup>2</sup> Center for Polymer Interface and Molecular Adhesion Science, Kyushu University, Fukuoka 819-0395, Japan

<sup>3</sup> Department of Materials Science and Chemical Engineering, Stony Brook University, Stony Brook, New York 11794-2275, United States

<sup>4</sup> Department of Chemistry, Stony Brook University, Stony Brook, New York 11794-3400, United States

<sup>5</sup> International Institute for Carbon-Neutral Energy Research (WPI-I2CNER), Kyushu University, Fukuoka 819-0395, Japan

Tel: +81-92-802-2879 (D.K.) and +81-92-802-2878 (K.T.)

E-mail: d-kawaguchi@cstf.kyushu-u.ac.jp (D.K.) and k-tanaka@cstf.kyushu-u.ac.jp (K.T.)

## 1. Experimental detail

### 1.1. Sample preparation and characterization.

Silicon wafers (SUMCO, Corporation, Tokyo, Japan) and half-cylindrical quartz prisms (Daiko MFG, Co. Ltd., Kyoto, Japan) were used as a substrate. They were cleaned by a piranha solution ( $\text{H}_2\text{SO}_4/\text{H}_2\text{O}_2$ , 70/30 v/v) at 373 K (100 °C) for at least 1 hour. The spinning rate and time were 3000 rpm and 60 s, respectively. The film thickness was controlled by varying the solution concentration.

Gel permeation chromatography (GPC) was conducted using HLC-8321GPC/HT (Tosoh, Co) with a set of three columns (TSKgel GMHHR-H, Tosoh, Co.). The eluent was 1,2,4-trichlorobenzene, and the column temperature was 413 K (140 °C).

**1.2 Sum frequency generation (SFG).** A visible beam with a wavelength of 532 nm was generated by frequency-doubling the fundamental output pulses from a picosecond Nd:YAG laser (PL2250-10-B, EKSPLA, Vilnius, Lithuania). A tunable infrared (IR) beam was generated from an EKSPLA optical parametric generation/amplification and difference frequency generation (OPG/OPA/DFG) system based on LBO and AgGaS<sub>2</sub> crystals. SFG spectra were collected with the visible and IR beams traveling through the prism and overlapping at the center of the sample. The incident angles for the visible and IR beams were 55° and 65° from the surface normal, respectively. The intensity of SFG signals ( $I^{\text{SFG}}$ ) is proportional to the square of the absolute value of the effective sum-frequency susceptibility tensor of the interface ( $\chi_{\text{eff}}^{(2)}$ ),

$$I^{\text{SFG}} \propto \left| \chi_{\text{eff}}^{(2)} \right|^2 I_{\text{vis}} I_{\text{IR}} \quad (\text{S1})$$

where  $I_{\text{vis}}$  and  $I_{\text{IR}}$  are the intensity of the visible and IR lasers, respectively. Thus, the intensity of the SFG signals was normalized by those of the original visible and IR beams. Here,  $\chi_{\text{eff}}^{(2)}$  can be described by the following equation,

$$\chi_{\text{eff}}^{(2)} = \chi_{\text{NR}}^{(2)} + \sum_q \frac{A_q}{\omega_{\text{IR}} - \omega_q + i\Gamma_q} \quad (\text{S2})$$

where  $\chi_{\text{NR}}^{(2)}$  and  $\omega_{\text{IR}}$  are the non-resonant background and the frequency of IR, respectively.  $A_q$ ,  $\omega_q$  and  $\Gamma_q$  are the peak intensity, resonant frequency and damping coefficient for the  $q^{\text{th}}$  vibrational mode, respectively. The peak intensity of each component was determined by curve-fitting using eqs. (S1) and (S2). The measurements were carried out at room temperature with the *ssp* (SF output, visible input, and infrared input) polarization combination.

**1.3 Grazing-incidence wide-angle X-ray diffraction (GIWAXD).** GIWAXD measurements were performed at the X9 beamline ( $\lambda = 0.0918$  nm and  $E = 13.5$  keV) at the National Synchrotron Light Source (NSLS), Brookhaven National Laboratory. Two-dimensional GIWAXD patterns were collected using a MAR-CCD area detector. The sample-to-detector distance was calibrated using a silver behenate standard sample. The incident angle ( $\theta_s$ ) of the X-ray was set to 0.11°, which was above the critical angle of isotactic polypropylene (*i*PP), hence illuminating the entire *i*PP film. All the results were collected at room temperature and each sample exposure time was fixed at 120 sec.

## 2. Details of analysis

**2.1 Orientation of (040) and (110).** Panels (a) and (b) of Figure S1 show the azimuthal angle ( $\phi$ ) dependence of intensity for the (040) and (110) reflections, respectively, extracted from Figure 1. Here,  $\phi$  was defined as the angle with respect to  $q_y$ . For the 180 nm-thick film, the (040) reflection was observed both around  $\phi = 0^\circ$  and  $90^\circ$ . On the other hand, the

reflection around  $\phi = 90^\circ$  disappeared for the 80 nm-thick film. As the film became thinner to 35 nm, the reflection at  $\phi = 0^\circ$  was sharper than that for the thicker films. These results indicate that the  $b$ -axis in the crystalline lamellae was more orientated along with the direction parallel to the substrate interface with decreasing film thickness. The (110) reflection was broadly distributed around  $\phi = 0^\circ$  and  $82^\circ$  for the 180 nm-thick film. This trend was also the case for the 80 nm-thick film. On the contrary, the reflection peak for the 35 nm-thick film became sharper and the center position for the off-axis reflection was shifted from  $82^\circ$  to  $73^\circ$ , as indicated by an arrow, although the peak at  $\phi = 0^\circ$  remained.

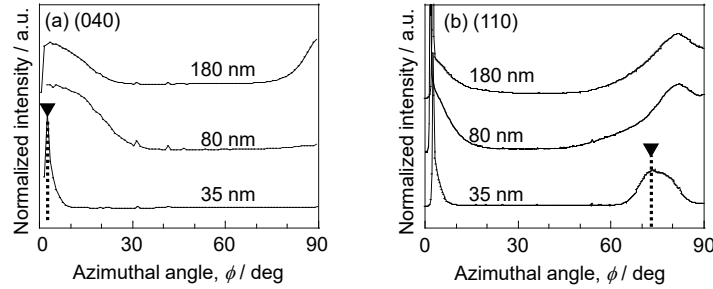


**Figure S1.** Azimuthal angle dependence of relative intensity of (a) (040) and (b) (110) reflections for *i*PP films of various thicknesses.

**2.2. Determining factors of lamellar orientation.** As a thermodynamic factor to determine the lamellar orientation, the free energy of a primary nucleus for edge-on and face-on lamellae at the surface and substrate interface was calculated.<sup>1, 2</sup> The difference of Gibbs free energy for the flat- and edge-on lamellae ( $\Delta G_F^* - \Delta G_E^*$ ) for *i*PP can be estimated on the basis of the surface free energies of the folding plane, crystal plane, supercooling melt, and substrate ( $\sigma_{eC}$ ,  $\sigma_C$ ,  $\sigma_M$ , and  $\sigma_s$ ).<sup>1</sup> The  $\Delta G_F^* - \Delta G_E^*$  is described by,

$$\Delta G_F^* - \Delta G_E^* = \frac{32(\sqrt{\sigma_{eC}} - \sqrt{\sigma_C})(\sqrt{\sigma_{eC}} - \sqrt{\sigma_M})(\sqrt{\sigma_C} - \sqrt{\sigma_M})^3(\sqrt{\sigma_s} - \sqrt{\sigma_M})}{\Delta f^2} \quad (S3)$$

where  $\Delta f$  is the free energy upon the crystallization per unit volume. In the case of the *i*PP film,  $\sigma_C$  and  $\sigma_M$  were  $11.5$ <sup>3</sup> and  $24.9$ <sup>4</sup>  $\text{mJ}\cdot\text{m}^{-2}$ , respectively, and  $\sigma_{eC}$  was larger than both  $\sigma_C$  and  $\sigma_M$ .<sup>2</sup> Also,  $\sigma_s$  for a Si wafer was calculated to be  $73.0$   $\text{mJ}\cdot\text{m}^{-2}$  based on the contact angle measurement. Thus,  $\Delta G_F^* - \Delta G_E^*$  is supposed to be negative at the silicon interface. This means that the face-on lamellae would be preferentially formed as the crystallization proceeded at the silicon interface. Assuming that the face-on mother lamellae were formed at first then branching of daughter lamellae occurred, our results can be explained in terms of the thermodynamic factor.

**2.3. Estimation of  $\chi^{(2)\text{eff}}$ .** To estimate  $\chi^{(2)\text{eff}}$ , at first, the refractive index ( $n$ ) of *i*PP was obtained from the literature. Masuko *et al.* experimentally determined the refractive index of biaxial stretching monoclinic *i*PP by combining X-ray diffraction, differential polarized infrared absorption spectrum, and birefringence.<sup>5</sup> As a result,  $n$  in the  $a$ -axis and  $c$ -axis directions were determined to be 1.51 and 1.54, respectively. They also formulated the  $n$  value ( $n_{\text{iso}}$ ) for *i*PP in an isotropic state as a function of the mass density ( $\rho$ ) of *i*PP,

$$(n_{\text{iso}} - 0.9353)/\rho = 0.6294 \quad (S4)$$

The  $n$  value for the amorphous region of *i*PP was estimated to be 1.47 using eq. (S4) and the  $\rho$  value of the amorphous ( $= 0.85 \text{ g}\cdot\text{cm}^{-3}$ ).<sup>6</sup>

The absolute value of  $\chi_{\text{eff}}^{(2)}$  of the interface for the *ssp* polarization condition can be expressed as follows;

$$\chi_{\text{eff}}^{(2)} = L_{yy}(\omega_{\text{SF}})L_{yy}(\omega_{\text{Vis}})L_{zz}(\omega_{\text{IR}}) \sin \theta_{\text{IR}} \chi_{yyz} \quad (\text{S5})$$

where  $L_{ii}(i = x, y, z)$  are Fresnel coefficients. The angle between surface normal and beam is expressed as  $\theta$ . The subscripts Vis and IR denote the input beams. To calculate Fresnel factors for the interfaces, the following equations are used,<sup>7</sup>

$$L_{xx}(\omega) = \frac{2n_1(\omega)\cos\theta_1}{n_2(\omega)\cos\theta_1+n_1(\omega)\cos\theta_2} \times \frac{2n_2(\omega)\cos\theta_2}{n_3\cos\theta_2+n_2(\omega)\cos\theta_3} \times \frac{\cos\theta_3}{\cos\theta_1} \quad (\text{S6a})$$

$$L_{yy}(\omega) = \frac{2n_1(\omega)\cos\theta_1}{n_1(\omega)\cos\theta_1+n_2(\omega)\cos\theta_2} \times \frac{2n_2(\omega)\cos\theta_2}{n_2\cos\theta_2+n_3(\omega)\cos\theta_3} \quad (\text{S6b})$$

$$L_{zz}(\omega) = \frac{2n_1(\omega)\cos\theta_1}{n_2(\omega)\cos\theta_1+n_1(\omega)\cos\theta_2} \times \frac{2n_2(\omega)\cos\theta_2}{n_3\cos\theta_2+n_2(\omega)\cos\theta_3} \times \frac{n_1}{n_3} \times \left(\frac{n_3(\omega)}{n'(\omega)}\right)^2 \quad (\text{S6c})$$

where  $n_i$  and  $\theta_i$  are the refractive index and the incidence angle in the medium  $i$ , respectively.  $n'$  is the refractive index of the interfacial layer which was an average value of the refractive indices of the two media. The  $\chi_{\text{eff}}^{(2)}$  values for each interface were calculated using eqs. S5 and S6 and  $n$  values.

## References

1. J.-P. Yang, Q. Liao, J.-J. Zhou, X. Jiang, X.-H. Wang, Y. Zhang, S.-D. Jiang, S.-K. Yan and L. Li, *Macromolecules*, 2011, **44**, 3511-3516.
2. K. Uchida, K. Mita, Y. Higaki, K. Kojio and A. Takahara, *Polym. J.*, 2019, **51**, 183-188.
3. E. J. Clark and J. D. Hoffman, *Macromolecules*, 1984, **17**, 878-885.
4. R.-J. Roe, *J. Phys. Chem.*, 1968, **72**, 2013-2017.
5. T. Masuko, H. Tanaka and S. Okajima, *J. Polym. Sci. Polym. Phys.*, 1970, **8**, 1565-1574.
6. J. Brandrup, E. H. Immergut and E. A. Grulke, *Polymer Handbook, 4th Edition*, Wiley, 2003.
7. H. Noguchi, M. Hiroshi, T. Tominaga, J. P. Gong, Y. Osada and K. Uosaki, *Phys. Chem. Chem. Phys.*, 2008, **10**, 4987-4993.